



A Fluvial Flood Risk Model for Quantifying the Benefit of Mitigation Measures under Uncertainty

Mara Ruf¹, Amelie Hoffmann¹, and Daniel Straub¹

¹Technical University Munich

Correspondence: Mara Ruf (mara.ruf@tum.de)

Abstract. We present a dynamic probabilistic flood risk model that addresses key challenges in the implementation of integrated flood risk management. These include the need for holistic, large-scale risk assessments that adopt a system-based perspective, and a decision-making framework based on benefit-cost analysis. The proposed model allows for the explicit simulation and dynamic coupling of the flood process components, including downstream flood wave propagation and possible dike failures, in a computationally efficient and data-sparse manner. It enables the consideration of aleatory and epistemic uncertainties in a 2-level Monte Carlo framework. By separating these uncertainties, the model supports robust risk assessments and facilitates the uncertainty-aware evaluation of the benefit of mitigation measures. The model is applied to the Bavarian Danube, demonstrating its ability to estimate the flood risk reduction potential from mitigation measures.

1 Introduction

- Over the past few decades, the approach to flood management has transitioned from a mainly technical focus on flood protection to a more comprehensive flood risk management strategy (Vitale, 2023; Thomas and Knüppe, 2016). This shift was catalyzed by significant flood events, such as the catastrophic 2002 flood in Central Europe, which traditional flood protection measures failed to prevent. With estimated direct damages of 22.6 billion Euros (reference year 2005; Petrow et al. (2006)), the 2002 flood stands as the most expensive natural hazard recorded in Germany. In response, numerous administrative and legislative initiatives were launched at both the EU and national levels to enhance preparedness for future flooding (Thieken et al., 2016). However, subsequent flood events in 2013, 2021, and 2024 have highlighted the need for further advancements in the implementation of integrated flood risk management, which can be summarized by three necessary key developments (Merz et al., 2010a):
- 20 1. Comprehensive risk assessment: While traditional engineering approaches relied on predefined design floods and corresponding protection levels (Messner et al., 2007), flood risk management encompasses the entire spectrum of potential flood events and their uncertain consequences. It acknowledges the possibility of flood protection failures, even below established design standards, and recognizes that absolute safety against flooding is unattainable. Deterministic models, which assume fixed relationships between return periods, water levels, and flood damage, are increasingly insufficient.



25

30

50

55



Recent studies have highlighted the downstream impacts of dike failures (Apel et al., 2009b; Curran et al., 2020). Consequently, flood risk assessments must explicitly model the flood process chain and dynamically couple its components. Different aleatory uncertainties exist in these components, which should, if possible, be represented in the model (Hall and Solomatine, 2008): Climate change affects both the frequency and magnitude of flood hazards, while uncertainties regarding dike breach resistance influence the likelihood of severe flooding in areas considered safe. Additionally, so-cioeconomic development impacts vulnerability. Alongside these aleatory uncertainties, epistemic uncertainties inherent in every flood risk model must be addressed. Numerous studies emphasize the critical role of these uncertainties in flood risk assessment (Hall and Solomatine, 2008; Dittes et al., 2018). There is a scientific consensus advocating for probabilistic approaches to enhance robust flood risk assessment and estimate the impact of uncertainties (Domeneghetti et al., 2013; Apel et al., 2004; Hall and Solomatine, 2008; Merz and Thieken, 2009).

- Shift in decision-making criteria: Decision-making processes must move from regulation-based frameworks to performance-based approaches, wherein the potential for flood risk reduction is weighted against the costs of mitigation measures (Messner et al., 2007). This criterion promotes a more transparent and cost-effective allocation of limited resources (Gamper et al., 2006). To evaluate the benefits of mitigation measures, flood risk must be estimated both with and without their implementation. Therefore, a model capable of simulating the impacts of mitigation measures at the site of implementation as well as downstream is essential. Both aleatory and epistemic uncertainties should be integrated and communicated within benefit-cost analyses (Hall and Solomatine, 2008). Decision-oriented sensitivity studies (Straub et al., 2025) can further enhance the decision-making process, ensuring robustness and transparency. While several studies (de Kok and Grossmann, 2010; Apel et al., 2006) have developed models that fulfill both the requirement of 1. Comprehensive risk assessment as well as 2. Shift in decision-making criteria, their integration into official practice is still lacking.
 - 3. Integrated, cross-border approaches: It is increasingly recognized that isolated, local flood protection strategies must be replaced by integrated approaches that frame flood risk mitigation as a comprehensive task spanning large spatial scales and involving multiple riparian communities (Thieken et al., 2016). Local flood mitigation efforts can have translocal consequences (Metin et al., 2018). Dikes may temporally and spatially shift flood hazard, potentially exacerbating flood risk downstream. Other flood protection measures, such as detention basins, are designed in a way that their impact propagates far downstream (Förster et al., 2005). Ignoring these interdependencies can undermine the optimal allocation of resources and diminish risk reduction potential. Moreover, integrated flood risk management encompasses not only technical solutions but also a diversification of management strategies, including spatial planning, early warning systems, nature-based solutions, and flood-proofing (Merz et al., 2010a). Despite decades of research advocating for integrated flood risk management, decision-making and its practical implementation often remain fragmented across various professional sectors that focus on local flood protection planning.

The transition towards integrated flood risk management requires a model capable of addressing the three critical developments outlined. The first probabilistic national-scale flood risk assessment in England was developed by Hall et al. (2003). In



80

85



this model, dike reliability is represented using fragility functions, which are coupled with a static inundation model to estimate expected annual flood risk across different regions. A basic uncertainty analysis is included to provide upper and lower bounds on the estimated risk. This methodology was further enhanced by Gouldby et al. (2008) at a regional scale, where the fragility functions were refined and hydraulic load scenarios probabilistically generated from extreme value distributions. However, both models lack dynamic coupling between components and, consequently, do not account for downstream discharge reductions following dike failures. Another model developed by Apel et al. (2004), applied to the Rhine River in North Rhine-Westphalia, Germany, incorporates hydrological load scenarios derived from a flood frequency curve, Muskingum-based flood routing, levee breach and outflow modeling as well as a static inundation and damage assessment. Dike failure due to overtopping is modeled using a 2D fragility function derived via Monte Carlo simulation of a limit state function under uncertain dike properties. However, breach assessment is limited to only two locations. Subsequent extensions of this model introduced uncertainty analysis (Apel et al., 2006) and allowed for quasi-continuous dike breach locations (Apel et al., 2009b). Similarly, the flood risk model developed by de Kok and Grossmann (2010) for the Elbe River in Germany integrates scaled synthetic flood events (based on predefined return periods), a dike breach module, a 1D hydraulic flood routing model, and a macro-scale economic damage assessment. Dike breaches are assumed to occur deterministically as a result of overtopping. While this approach allows for scenario-based risk assessment, it does not include a formal uncertainty analysis. More recently, the Germany-wide flood risk assessment by Sairam et al. (2021) employs a flood event catalog derived from 5,000 years of hydro-meteorological simulation data, coupled with a 1D-2D hydrodynamic model to simulate flood propagation and inundation as a consequence of dike overtopping. Dike failure and its consequences are not included, but a comprehensive uncertainty analysis is conducted. The flood hazard model of Apel et al. (2009a) was further refined by Vorogushyn et al. (2010) and extended by the failure mechanisms piping and micro-instability. Moreover, the original flood routing approach was replaced with a 1D hydrodynamic simulation, and the inundation assessment upgraded to a 2D storage-cell-based hydrodynamic model. These enhancements necessitate runtime coupling of the probabilistic model with process-based simulations, increasing the degree of process representation. Domeneghetti et al. (2013) applied this advanced model to a 50 km reach of the Po river in Italy, demonstrating its capability for probabilistic flood hazard mapping under uncertainty. The comparative analysis of all these works emphasizes the trade-off in large-scale flood modeling between accurate process representation, broad spatial coverage, and comprehensive integration within uncertainty analyses.

In this work, we introduce a novel probabilistic flood risk model that dynamically couples process components at runtime (Fig. 2). The model enables the assessment of flood risk as well as flood risk reduction potential of mitigation measures, accounting for inherent uncertainties in flood hazard and explicitly considering the potential for dike failures. The central advantage of the model is its computational efficiency, which facilitates a comprehensive uncertainty analysis. This is achieved through diverse pre-processing simulations that decouple the model at runtime from computationally expensive hydraulic and hydrodynamic simulations. Essential to this decoupling is a flood routing method that efficiently captures the downstream propagation of dike failures and mitigation impacts. The flood risk model is embedded in a 2-level Monte Carlo framework, where aleatory and epistemic uncertainties enter separately, which supports robust decision-making processes. Ultimately, the flood risk model promotes integrated, cross-border decision-making by enabling direct integration into benefit-cost analyses of







Figure 1. Overview of the study area.

mitigation measures. The model is currently implemented for the Bavarian Danube to evaluate the benefit of flood mitigation measures. Section 2 introduces the study area. Section 3 outlines the various flood components and their integration in the developed flood risk model. Section 4 presents the model's incorporation into a two-level Monte Carlo framework. Illustrative results are provided in Section 5.

2 Study area

100

105

The study area utilized in this work to develop, test and demonstrate the application of the flood risk model is the Bavarian part of the Danube River, Germany, shown in Fig. 1. The Danube originates in Baden-Württemberg in western Germany, flowing for approximately 380 km through Bavaria before crossing the border into Austria, east of Passau. The river's hydrology is heavily influenced by its tributaries, many of which originate in the Alps, including the Iller, Lech, Isar, and Inn rivers. In addition, the northern catchment area is fed by key tributaries such as the Wörnitz, Altmühl, Naab, and Regen rivers, which arise in the Central German Uplands. Notably, flood dynamics in the northern and southern catchment areas of the Danube differ in terms of underlying formation mechanisms and seasonal patterns, which, in turn, affect flood wave characteristics. This plays an important role in shaping the overall flood hazard associated with the Bavarian Danube. Approximately 54% of the catchment area is used for agriculture, 34% is covered by forests, and 13% is urbanized. Significant industrial centers, including Donauwörth, Ingolstadt, and Regensburg, are located along the river. The cities Regensburg and Ingolstadt are the third and fourth most populous cities in Bavaria.

110 3 Flood risk model

The developed flood risk model comprises five primary modules that collectively represent the flood process chain: the hydrological load module, the dike failure module, the hydrodynamic module, the inundation module, and the damage module.



115

120

125

130



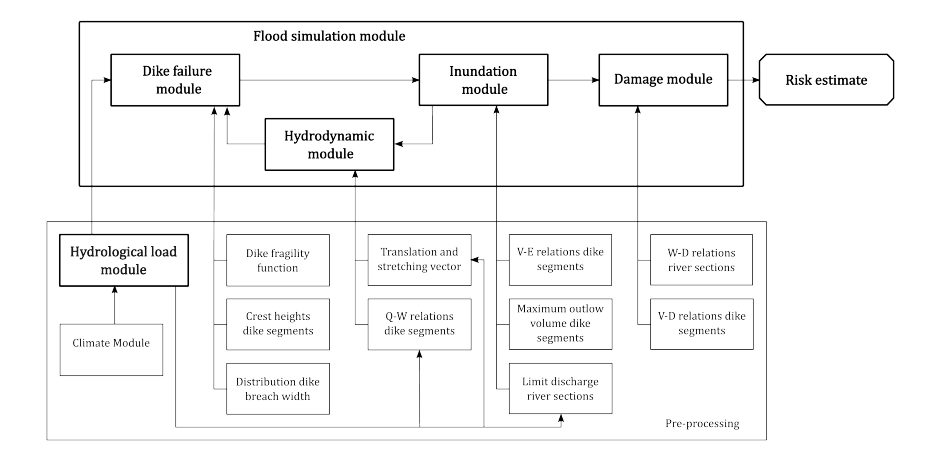


Figure 2. Schematic overview of the flood risk model.

Among these, the dike failure, hydrodynamic, and inundation modules are dynamically coupled to enable updates between them during simulation runs. The flood risk model is summarized in Fig. 2 and further explained in the following sections. It is integrated within a 2-level Monte Carlo framework, which distinguishes between aleatory and epistemic uncertainty (see Section 4). To optimize computational efficiency, all modules utilize pre-computed runs from various modeling tools, as indicated by the pre-processing box in Fig. 2.

To apply the flood risk model to a specific case study, several preparatory steps must be undertaken. Although these steps are exemplified for the Bavarian Danube study area, they can be easily adapted to other catchments. First, the river and its surrounding foreland are contained on both sides by a longitudinal embankment line. In areas where river dikes exist, this embankment line coincides with their alignment; in other locations, it follows the border of the 100-year event. Second, the river and its longitudinal embankment line are laterally discretized into sections ranging from 300 to 600 m in length, following the recommendations of CUR/TAW (1990). This choice ensures that the response of dikes of this length to hydraulic loading is approximately independent of its neighbours (Vorogushyn et al., 2010). Additionally, the river reach is longitudinally divided into two parts to model river bifurcations. As a result of this discretization process, a total of 2x892 river segments are defined along the Bavarian Danube. The adjacent longitudinal structures are termed embankment segments, which are further categorized as either dike or non-dike segments. Dike segments with overlapping hypothetical inundation areas are grouped together into impact zones. Figure 3 illustrates the spatial structure of the model. The segmentation and zoning enable efficient modeling of the flood process but introduce model inaccuracies, such as the overestimation of water heights when flooding exceeds the extent of the 100-year event.

3.1 Hydrological load module

Flood hazard can be characterized by a range of representative flood scenarios, each associated with a specific occurrence probability. The derivation of these flood scenarios can be accomplished through various approaches. While early flood risk



135

140

145

150

155



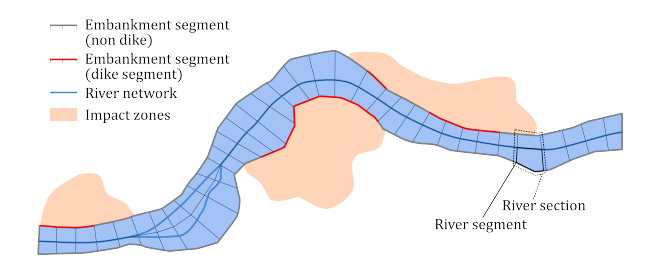


Figure 3. Schematic spatial discretization structure of the river.

assessments predominantly relied on historical or design hydrographs, these approaches have mostly been replaced by the synthetic generation of flood waves based on (multi-variate) distributions (Curran et al., 2020) or climate-based precipitation simulations (Sairam et al., 2021). Methods that depend on historical observations often face challenges in extrapolation, particularly when predicting flood events and their probabilities beyond the range of observed data. Various extreme value statistics and clustering methods have been employed in the literature to derive synthetic hydrographs based on flood frequency analyses (Vorogushyn et al., 2010). By contrast, climate-based precipitation simulations are theoretically independent of specific historical flood events and thus offer the greatest potential for representing flood hazard beyond the range of observed records (Ludwig et al., 2019). Simulated flood events often undergo post-processing—such as rescaling or adjustment of occurrence rates—for bias correction based on historical observations; in practice, they are not entirely independent of past events. Furthermore, these simulations are computationally demanding and susceptible to systematic errors if not rigorously calibrated.

In the current study, a set of flood events is derived from the ClimEx project, which conducted quasi-random, climate-based simulations of hydrometeorological events in Bavaria (Ludwig et al., 2019). A total of 50 transient simulations over the time horizon of 1980 to 2099 were carried out, employing the IPCC emission scenario RCP8.5 (IPCC, 2013). From these simulations, 3,500 years of precipitation data covering the period from 1980 to 2050 are extracted. Hence, the selected precipitation events reflect the climatic conditions of the recent past, present, and the near future relative to the reference year 2020 of the study. The decision to exclude simulations beyond this period is based on the significant uncertainties associated with future climatic conditions and their potential impact on precipitation patterns. Following intermediate simulations of runoff generation using WaSim (Schulla and Jasper, 2007) and flood routing within the catchment via Larsim (Bremicker, 2000), 72 flood events are identified that exceed a 100-year event on at least one of the gauging stations along the Bavarian Danube. The detention basin evaluated in this study (5 is designed to be activated only when the discharges exceed the threshold of a 100-year event. Consequently, the identified flood events can be interpreted as Monte Carlo samples of flood occurrences for which the evaluated measure provides a benefit, representing the aleatory uncertainty (randomness) associated with the flood event. The occurrence rate of these flood events is estimated as $\lambda = 72/3,500 \text{ years}^{-1}$. If measures are examined that already take effect at lower discharge thresholds, the flood event catalog must be extended accordingly. The 72 flood events are subsequently routed through the Danube River channel using the 1D non-stationary hydraulic modeling tool SOBEK (Deltares, 2018). Each river segment is linked to a hydraulic SOBEK node, ensuring that the flood events are spatially discretized according to the





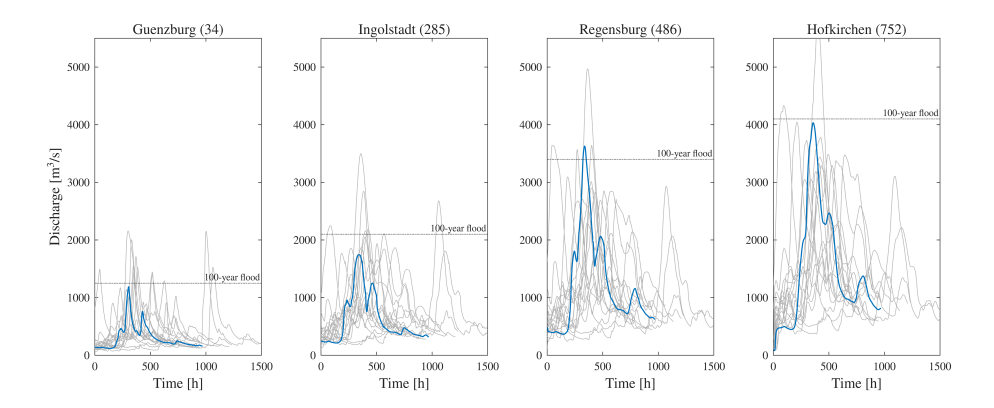


Figure 4. Hydrograph of 19 exemplary flood events at four locations along the Bavarian Danube. Segment number of location in brackets. One randomly chosen flood event is shown in blue.

model's resolution. A temporal resolution of one hour is used in the flood risk model. In case of unbifurcated river reaches, the two segments of a river section are linked to the same SOBEK node; for the bifuricated case, different nodes are assigned to the two opposite segments of a river section. For illustration, 19 flood events are depicted in Fig. 4 at four exemplary segments along the Bavarian Danube.

In addition to discharges Q along the river network, the hydraulic simulations provide corresponding absolute and relative water levels W. For each river segment, an empirical stage–discharge relationship is derived by binning simulated Q–W pairs from all flood events based on discharge values. Within each bin, mean discharge and water level values are calculated to construct a discretized stage-discharge curve. In the flood simulation model, water levels are then estimated via piecewise linear interpolation between these values. While computationally efficient, this method assumes a single-valued Q–W relationship and therefore does not capture hysteresis effects.

170 3.2 Dike failure module

165

175

180

Dikes are most likely to fail when water levels significantly exceed design specifications. In this study, failure refers to the physical breach or collapse of the dike, while overtopping denotes the overflow of water across the dike crest without implying structural damage. Failure resulting from overtopping is implicitly accounted for through the fragility function, as outlined below. Dike failures can result in catastrophic damage, especially when affecting densely populated areas, a phenomenon often referred to as the "levee effect". Studies have extensively investigated the relationship between dike breaches and flood damage, underscoring the importance of understanding dike reliability (Vorogushyn, 2008; Curran et al., 2019; Gouldby et al., 2008). The reliability of dike systems can be assessed through three primary approaches: empirical analyses, expert judgment, and model-based probabilistic analyses (Schultz et al., 2010). First efforts to systematically quantify the probability of dike failure using fragility functions were made by the U.S. Army Corps of Engineers in the early 1990s (USACE, 1991). Since then, considerable research has been conducted, and model-based probabilistic approaches have gained significant traction in the field. Dike failure modes can be categorized into three primary types: hydraulic, geohydraulic, and global static failure



185

190

195

200

205

210



(Vorogushyn, 2008). Hydraulic failure occurs when overtopping water erodes the dike material from the landward side. If wave-induced overtopping is neglected — an assumption adopted by Vorogushyn (2008); Apel et al. (2004); Domeneghetti et al. (2013) — the probability of hydraulic failure is zero for water levels below the dike crest height. Geohydraulic failure arises from an uplift of the dike core, typically resulting from piping processes occurring in the dike foundation. In contrast, global static failure is induced by microinstability within the dike core due to internal seepage processes. A comprehensive study of the analytical description of dike failure modes was conducted by Vorogushyn (2008).

Vorogushyn (2008) describes the physical processes leading to failure through the use of limit state functions, which typically compare the stress S acting on a structure with its resistance R: g(R,S) = R - S. Failure occurs if $g(R,S) \le 0$, i.e., when S exceeds R. Both R and S are treated as uncertain and are characterized by a range of random variables corresponding to different dike properties. For the three distinct failure modes, different (conditional) sub-mechanisms are incorporated into the limit state function. In this work, the limit state functions for the (sub-)mechanisms contributing to g(R,S) are derived from the work of Vorogushyn (2008) and evaluated using a Monte Carlo simulation to generate fragility functions. For all random variables entering q(R,S) for which no site-specific data was available, probability distributions are based on Vorogushyn (2008). The resulting conditional failure probabilities are in function of various load variables, such as water level relative to crest height, overtopping duration, and impoundment duration. To reduce computational complexity and streamline the model, these variables are not directly evaluated in the flood simulation model. Instead, the fragility functions are evaluated in a preprocessing step at each dike segment independently, utilizing the flood events outlined in the hydrological load module in Section 3.1. By calculating the expected value of the failure probability conditional on the maximum water level relative to the crest height h_k of each dike segment, a fragility function is obtained that is conditional solely on the relative water level. This function incorporates all three failure mechanisms and implicitly contains information regarding the characteristics of the underlying flood scenarios. Hence the fragility function is specific for the considered study area and flood events. It is presented in Fig. 5.

In the flood simulation model, the fragility function is applied to each dike segment. A breach resistance value — defined as the maximum water level the segment can withstand before failure — is randomly sampled from the fragility function. The resistances of dike segments are considered independent of one another, justified by the rationale for the choice of segment length outlined in Section 3. Dike failure is defined to occur when the water level, at any time during the flood event, exceeds the breach resistance. In case of breaching, the breach width b is quasi-randomly sampled from a lognormal distribution with parameters $\mu_b = 58.5$ m and $\sigma_b = 61.3$ m, following Vorogushyn (2008). If the sampled breach width falls outside the range $[3 \text{ m}, b_s]$, with b_s equal to the segment width, it is truncated to conform to these limits. Thus, both breach resistance and breach width — and therefore the aleatory uncertainties inherent in the breaching process — are accounted for by the Monte Carlo simulation. The breach development rate is assumed to be one hour, consistent with the methodology employed by Apel et al. (2004, 2006) and Vorogushyn (2008). The breach is assumed to erode the entire dike down to the toe level of the dike, h_t .





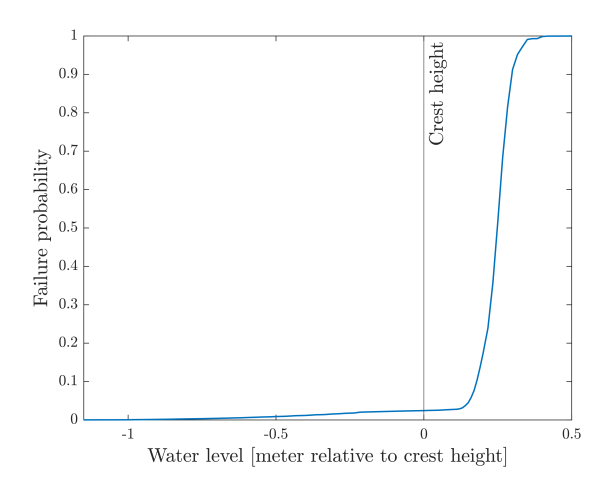


Figure 5. Developed fragility function for single dike segments. This function is specific to the case study.

3.3 Inundation module

220

225

230

The hourly outflow discharge through the dike breach (or overflow over the crest in the absence of failure) into the hinterland at time step t is calculated using a modified broad-crested weir equation:

$$Q_{out}(t) = 2/3 \cdot \mu_0 \cdot \mu^* \cdot \sqrt{2g} \cdot b \cdot h^{3/2}(t)$$
(1)

where g [m/s²] is the gravitational force, h [m] the overfall height, $\mu_0 = 0.577$ [-] the flow factor and $\mu^* = 0.7$ [-] a discharge reduction factor to account for the influence of the dike breach, motivated by the studies of Kamrath et al. (2006). The overfall height is

$$h(t) = \begin{cases} h_t + w(t) \text{ for breaching} \\ w(t) - h_c \text{ for overtopping} \end{cases}$$
 (2)

with h_t and h_c the height of the dike toe and dike crest respectively, and w(t) the water level in the river segment. Discharge over the dike crest or through the dike breach is constrained. For each river segment, a limit discharge remaining in the river channel Q_l at both dike crest height and dike toe height is estimated in a pre-processing step based on the Q-W relationship obtained from the hydraulic simulation discussed in Section 3.1. With $Q_{out}(t) = \min\{Q_{out}(t), Q_{river}(t) - Q_l\}$, it is ensured that the outflow does not exceed physically plausible limits, neglecting wave influence. Additionally, w(t) in the river segment is compared to the inundation elevation in the hinterland $E_{in}(t)$ at the respective time step. Consequently, the model automatically switches between free and drowned overfall, depending on the water levels in the river and the hinterland. The outflow volume V(t) is approximated as the sum of the outflow discharges $V(t) = \sum_{t'=1}^{t-1} Q_{out}(t') \cdot 3600$ s. Backwater discharges are not modeled directly; rather, the outflow volume is constrained by a segment-specific maximum volume V_{max} determined by the topography and the surrounding dike heights, which is further outlined below.



235

240

245

250

255

260

265



Inundation modeling aims at estimating the extent of flooding given the topography and the boundary conditions of the breach and can be conducted with varying degrees of detail. The choice depends on the available computational and data resources, the objectives and scale of the study area, and the level of detail of other components of the flood risk model. In their national-scale flood risk assessment, Hall et al. (2003) estimated flood extent using a simple approximation method, spreading the calculated flood volume while assuming an average flood depth and a semi-circular or trapezoidal outline shape. de Kok and Grossmann (2010) utilized pre-computed volume-storage functions based on a 100x100 m grid to determine inundation depths. For their study at the Rhine River in Germany, Apel et al. (2004, 2006) derived so-called damage functions prior to the Monte Carlo simulation, assuming a horizontal filling of the hinterland in 0.5 m increments. This approach involved intersecting a horizontal plane with the digital elevation model (DEM). Vorogushyn et al. (2010) simulated the inundation process at run time using a 2D raster-based diffusive wave model that solves the continuity and momentum equations. This study employed a DEM with a 50x50 m grid cell resolution and average, land-use-specific roughness values based on literature data. A similar approach was pursued in the Italian flood hazard study conducted by Domeneghetti et al. (2013) at the Po River.

In this work, the relationship between inundation elevation (E) and inundation volume (V) is derived statically for each dike segment using ArcGIS. The developed method iteratively performs intersections between a 5x5 m digital elevation model (DEM) and horizontal surfaces at 0.1 m height increments. As a constraint, the algorithm assesses the connectivity of the resulting surfaces with their corresponding dike segments, systematically removing any disconnected islands. Additionally, inundation areas are cut along tributaries. Five resulting inundation areas at breach segment 500 are depicted in Fig. 6. As a result, V-E tables and hypothetical inundation areas are created for each segment. Furthermore, segments with overlapping hypothetical inundation areas at reasonably high inundation elevations are grouped together into impact zones. To account for backwater effects, the maximum outflow volume for each dike segment V_{max} is derived based on a simple approximation. This is achieved by considering the terrain slope in the direction of river flow, the height of the downstream protective structures within the same impact zone, and the derived V-E relationship. Additionally, in case of several breaches in a single impact zone, it is assumed that water flows together and forms one inundation area. Hence, the sum of the individual outflow volumes is used for inundation elevation and damage estimation. Elevation and damage (D) estimations are conducted based on the V-E and V-D (see Section 3.5) relationships of all involved segments using the total volume. The lowest resulting elevation and the highest damage estimate are chosen as decisive. Exemplarily, the resulting relationship between volume V and elevation Efor segment 500 downstream of Regensburg is depicted in Fig. 9. In analogy to the dike segments, inundation areas are derived for all river sections. As a constraint in the GIS-based derivation of inundation areas for river sections, the algorithm assesses the connectivity of the inundation surfaces with the river network.

The simplified static approach offers the advantage that, in case of breaching or overtopping, no process-based simulation of the flood wave in the hinterland is needed. Instead, a computationally inexpensive interpolation is conducted for each time step of outflow discharge. However, this approach neglects the influence of various parameters such as terrain roughness, flow velocity, flow direction, and settlement structures on the propagation of the flood wave. The impact of these simplifications varies depending on the existing topography, as studied by Apel et al. (2009a). Generally, it can be assumed that water depths





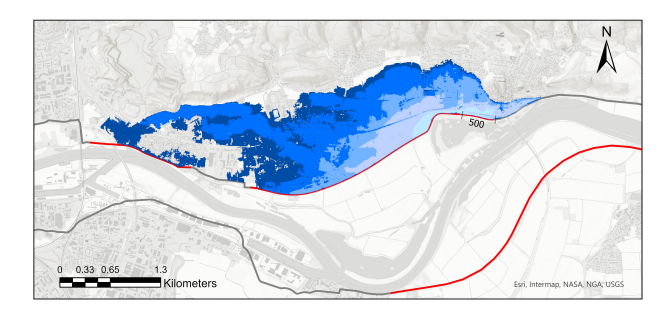


Figure 6. Five exemplary inundation areas at breach segment 500 derived with static GIS approach. Inundation elevations are: 328, 329, 330, 331 and 331.8 meters.

may be overestimated. However, Apel et al. (2009a) concluded that the consequences of the inaccuracies resulting from static inundation modeling are small compared to those resulting from large-scale damage assessments.

3.4 Hydrodynamic module

270

275

280

285

The influence of dike breaches on downstream flood hazard has been emphasized in several studies over the past two decades, e.g., Vorogushyn (2008); Curran et al. (2019); Apel et al. (2009b). If not properly incorporated, the downstream flood hazard can be significantly overestimated. At the same time, flood protection measures, such as detention basins, are designed in a way that they take effect until far downstream (Förster et al., 2005). This influence of mitigation measures and their possible failure on the flood hydrographs at downstream locations is modelled using a flood routing technique. Flood routing can be incorporated into flood risk models in varying degrees of detail. de Kok and Grossmann (2010) employ an empirical quick routing model that multiplies the discharges by a dimensionless system function. This system function depends on the length of the river segment, as well as translation and diffusion coefficients. Apel et al. (2004) apply the Muskingum method for flood routing, estimating travel time and form parameters based on 1D hydraulic simulations. Vorogushyn et al. (2010) utilize an unsteady 1D hydrodynamic model based on the Saint-Venant equations and cross-sectional profiles for river flood routing.

In this work, a vector-based flood routing approach is developed, which is composed of a translational and attenuation vector. It efficiently updates temporally and spatially discretized discharges downstream of a failed dike or an activated detention basin. The derivation of translational and attenuation vector is calibrated with the hydraulic modeling outcomes of the 1D simulation, conducted in the scope of Section 3.1. The translational vector is defined as $\mathbf{T} = (T_1, T_2, \dots, T_n) \in \mathbb{N}_0^{1 \times n}$, where n = 892 is the total number of river segments. Each entry T_i represents the mean travel time from the reference section 1 to segment i. \mathbf{T} is derived from a set of $N_{sim} = 18$ hydraulic simulations, where artificial discharge reductions are applied to the flood hydrographs at the most upstream segment, resulting in N_{sim} discharge matrices $\mathbf{Q}_{red}^{(k)} \in \mathbb{R}^{N_t \times n}$. N_t is the number of time steps in the flood scenario k. For each flood simulation k, the discharge reduction $\Delta \mathbf{Q}_i$ at segment i is defined as:

$$\Delta \mathbf{Q}_i^{(k)} = \mathbf{Q}_i^{(k)} - \mathbf{Q}_{\text{red},i}^{(k)},\tag{3}$$





where $\mathbf{Q}_i^{(k)} \in \mathbb{R}^{N_t \times 1}$ is the original discharge matrix of scenario k at segment i. The time of maximum discharge reduction $t_i^{(k)}$ is extracted for each segment i:

290
$$t_i^{(n)} = \arg\max_t \left\{ \Delta Q_i^{(k)}(t) \right\}$$
 (4)

A sliding-window median filter is applied to $\{\mathbf{t}^{(k)}\}$ for all simulations k, resulting in $\tilde{\mathbf{t}}^{(k)}$. The final translational vector entries $T_i \in \mathbf{T}$ are computed as the mean of the median-smoothed values over all flood scenarios:

$$T_i = \frac{1}{N_{sim}} \sum_{k=1}^{N_{sim}} \tilde{t}_i^{(k)} \tag{5}$$

In the flood simulation module, the relative travel time between a breach segment b and a downstream segment i is then computed as

$$T_i^{(rel)} = T_i - T_b \tag{6}$$

Given a computed discharge reduction $\Delta \hat{\mathbf{Q}}_b \in \mathbb{R}^{N_t \times 1}$ at the breach location b, the corresponding discharge reduction without retention and attenuation effects at each downstream segment i is computed by time-shifting $\Delta \mathbf{Q}_b$ according to the relative travel time $T_i^{(rel)}$, and applying the reduction across the relevant time steps t:

300
$$Q_i^{(k)}(t) - \Delta \hat{Q}_b(t - T_i^{(rel)}), \quad \text{for all } i > b \text{ and } t \in [t_B + T_i^{(rel)}, t_B + T_i^{(rel)} + N_{t_R}],$$
 (7)

where t_B is the time instance of breaching and N_{t_B} the duration of breaching. To model retention and attenuation effects, an attenuation vector is defined as

$$\mathbf{A} = (A_1, A_2, \dots, A_n) \in \mathbb{N}_0^{1 \times n},\tag{8}$$

where each entry A_i represents the temporal spread of the discharge reduction at segment i. For each segment i, the attenuation factor A_i defines a symmetric temporal window of size $\tau_i = 2 \cdot A_i + 1$. The discharge reduction is then redistributed evenly across this window:

$$\hat{Q}_{red,i}(t) = Q_i^{(k)}(t) - \sum_{i=-A}^{A_i} \frac{1}{\tau_i} \cdot \Delta \hat{Q}_b(t+j-T_i^{(rel)}), \quad \text{for all } i > b \text{ and } t \in [t_B + T_i^{(rel)}, t_B + T_i^{(rel)} + N_{t_R}]$$
(9)

This operation preserves the total reduction volume while approximating the attenuation observed in the hydraulic simulations. The attenuation vector \mathbf{A} is composed of a generic, segment-independent component \mathbf{A}_g , and a segment-specific component \mathbf{A}_s . The attenuation vector entry i given a discharge reduction at a location b is calculated as





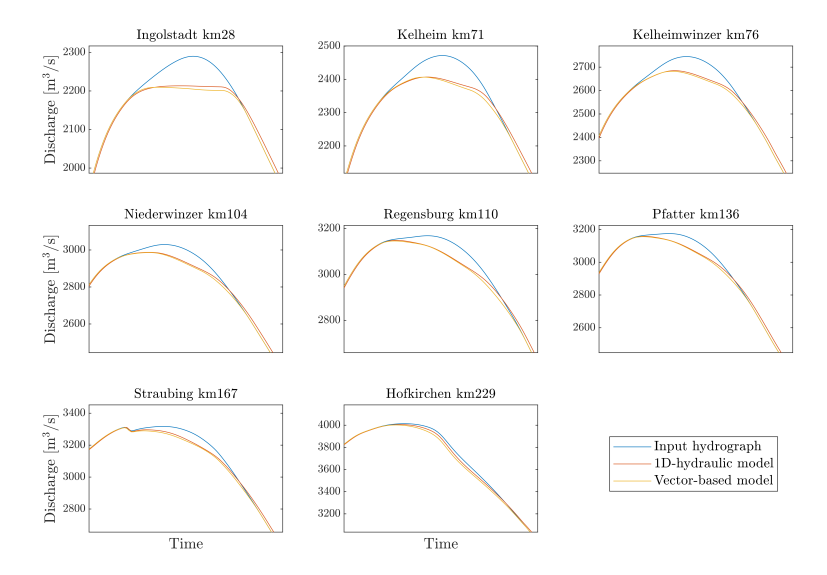


Figure 7. Comparison of 1D hydraulic SOBEK model results and vector based approach at 8 different locations. Kilometer values indicate distance to discharge reduction section. In blue: Uncapped input hydrograph, in red: propagated discharge reduction using 1D hydraulic model, in yellow: vector-based discharge reduction propagation.

$$A_i = A_{g,i} + A_{s,i} - A_{s,b} (10)$$

To derive the attenuation vector components, a set of $N_{sim}=18$ additional hydraulic simulations are performed, where artificial discharge reductions are applied at different locations in the river network. The optimal attenuation vector components $A_{g,i}^{(opt)}$ and $A_{s,i}^{(opt)}$ for each segment i are determined through a parameter search procedure that minimizes the global error between the 1D hydraulic model and the translated and attenuated discharge reductions applying the vector-based approach across all scenarios for a range of candidate values:

$$[\mathbf{A}_{g}^{(opt)}, \mathbf{A}_{s}^{(opt)}] = \frac{1}{N_{sim}} \sum_{k=1}^{N_{sim}} \arg\min_{\mathbf{A}_{g}, \mathbf{A}_{s}} \left\{ \sum_{t=1}^{N_{t}} \sum_{i=1}^{n} \left(\mathbf{Q}_{red}^{(k)}(t, i) - \hat{Q}_{red}^{(k)}(t, i) \right)^{2} \right\}$$
(11)

The vector-based flood routing approach is tested using an independent set of 40 1D hydraulic simulations, in which the peak discharge is reduced by 8 million m³ at the location of the detention basin at segment 216, which is introduced in Section 5. The comparison of one resulting set of hydrographs at eight downstream segments is presented in Fig. 7.

Differences in peak discharge ΔQ relative to the vector-based peak discharge, temporal offset of peak discharge, ΔT , absolute difference in peak water level, ΔW , as well as the continuous Nash-Sutcliffe-Efficiency (NSE) criterion are evaluated



330



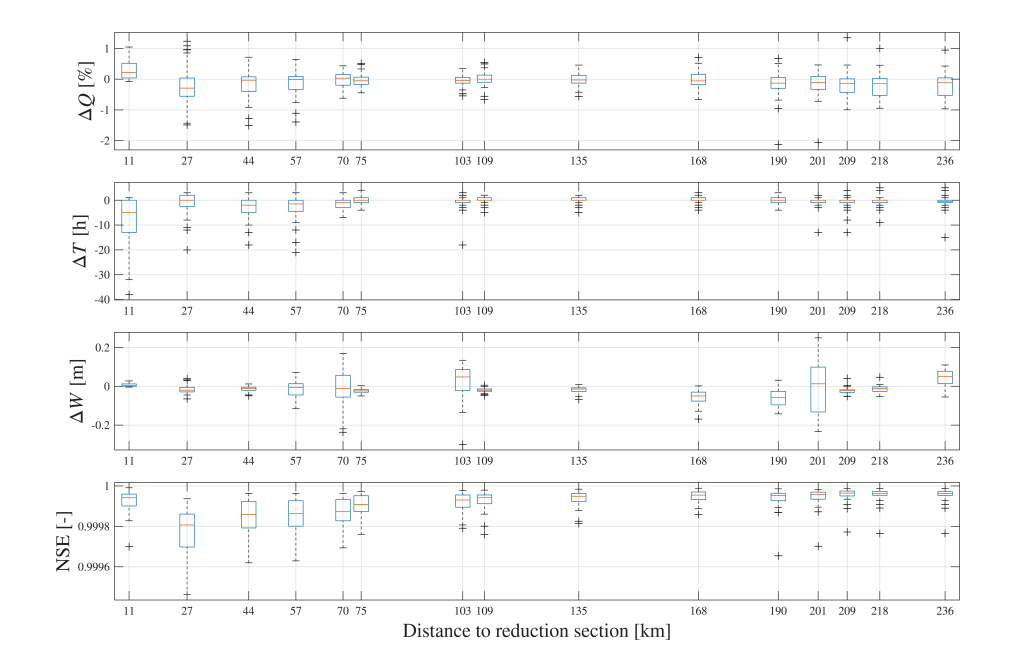


Figure 8. Quality criteria of vector-based flood routing approach, evaluated at 15 downstream segments. ΔQ refers to the difference in peak discharge between vector-based and 1D hydraulic simulation relative to the absolute peak discharge in the 1D simulation. ΔT is the temporal offset of the peak discharge [h], ΔW the absolute difference in peak water level [m], NSE the Nash-Sutcliffe-Efficiency of all discharge times series of the vector-based approach compared against the 1D hydraulic simulation.

at 15 downstream gauges for all 40 flood scenarios. The NSE is defined as

$$NSE = 1 - \frac{\sum_{t=t_{startfill}}^{N_t} (Q_{ref}(t) - Q_{model}(t))^2}{\sum_{t_{startfill}}^{N_t} (Q_{ref}(t) - \overline{Q_{ref}(t)})^2}$$
(12)

where model indicates the results of the vector-based propagation approach, ref those of the 1D hydraulic simulation that serve as the reference, $t_{startfill}$ the first time instance at which the detention basin is filled (and the discharge downstream reduced) and N_t the total number of time steps. The resulting statistics of the quality criteria are shown in Fig. 8. They indicate that the differences between the hydraulic and vector-based routing results are low, especially compared to the discrepancy between the 1D and 2D hydraulic simulations.

At bifurcation points, where the river splits into multiple reaches, the vector-based routing approach does not explicitly resolve travel time or retention differences between the diverging paths. However, discharge reductions must be accurately partitioned between downstream reaches. To achieve this, a main reach and a threshold discharge \mathbf{Q}_{th} are defined at each bifurcation segment. Secondary reaches are activated only when the local discharge exceeds \mathbf{Q}_{th} . The distribution of the discharge reduction is then determined using lookup tables \mathbf{Q}_{share} , derived from the hydraulic simulations in Section 3.1. For each bifurcation segment, Q_{share} maps the effective discharge $Q_{eff}(t) = Q(t) - Q_{th}$ to a discharge split ratio across the available reaches. This ensures that discharge reductions are apportioned consistently with observed flow behavior in the hydraulic model.



340

345

350



3.5 Damage module

Flood damages can be classified into direct and indirect damages and further subdivided into tangible and intangible damages (Merz et al., 2010a). The proposed flood risk model primarily addresses tangible damages. Considerable research has been conducted on direct tangible flood damage estimation, resulting in the introduction of various methodologies in recent years. Factors such as available data, understanding of damaging processes, study scale, and computational resources may limit the accuracy of direct tangible damage assessments. The general procedure for tangible flood damage assessment can be outlined in three steps (de Moel et al., 2015; Messner et al., 2007): 1) classification of elements at risk, 2) exposure analysis estimating the number, type, and asset value of these elements, and 3) vulnerability analysis, which evaluates the relative damages of exposed assets given the flood impact.

- 1. In large-scale flood risk analyses, elements at risk are typically grouped into classes. Within a class, all elements are treated uniformly; for example, their vulnerability to flooding is assumed to be identical. The number of groups and the corresponding detail of the classification depend on the study's scale and objectives, the significance of the objects within each class, data availability, and computational resources. In flood risk studies, classification is commonly based on land-use classes.
- 2. The exposure analysis identifies elements at risk from flooding. This is typically achieved by intersecting land-use data (or other class data) with inundation data using geographic information systems. Disaggregation may be necessary when class polygons are large.
- 3. Damage functions relate the (relative) damage within an asset class to specific intensity parameters. The most frequently used intensity parameter in flood damage assessments is inundation depth; however, other parameters, such as flow velocity, duration of inundation, contamination, and time of occurrence, also affect the losses. Neglecting these parameters may lead to significant overestimations of water depths and inundation extent, as highlighted in Section 3.3, which in turn can lead to overestimated damages. Nevertheless, such simplifications are frequently made due to data or computational constraints. Damage functions can be derived through empirical or synthetic approaches (Merz et al., 2010a). A wide variety of different damage functions for the same asset classes exists in the scientific literature, as well as in flood risk management and insurance practices, indicating substantial uncertainties at this stage (Messner et al., 2007). When selecting a damage function, it is crucial to ensure compatibility between asset classes and the corresponding damage functions.

The damage assessment approach employed in this study aligns with the established three-stage methodology. Damage classes are assigned based on the land-use classifications utilized in the Basic European Assets Map (BEAM) (geomer GmbH and Ruiz Rodriguez + Zeisler + Blank GbR, 2020). This map comprises 12 land-use classes, which are further subdivided into asset classes to facilitate more precise asset assessment. BEAM is composed of polygons based on the underlying land use structure. A land use class and relative asset value [EUR/m²] is assigned to each polygon. For every inundation area, a GIS-based intersection is conducted between the DEM, BEAM polygon layer, and the inundation polygon. For every grid cell



385



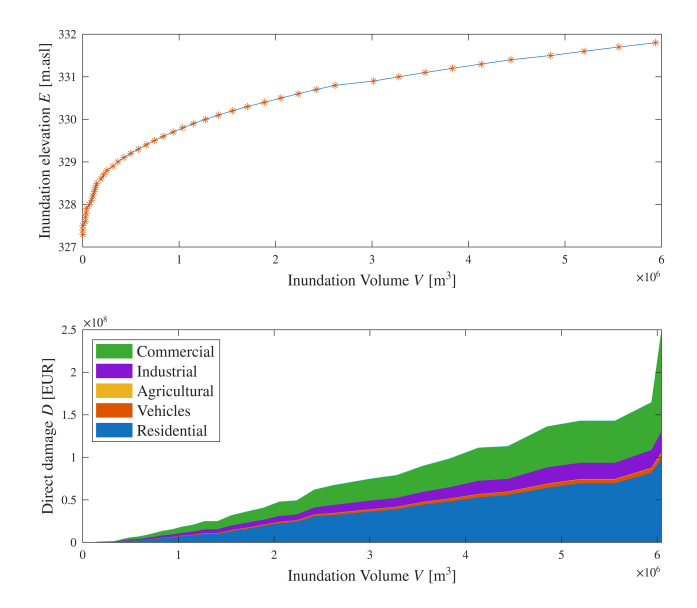


Figure 9. Relation between volume and elevation (upper) and volume and damage (lower) of dike segment 500 (left river side).

of the DEM, the height difference between the DEM and the inundation polygon is calculated, referred to as water depth. To optimize computational efficiency, water depth is discretized into intervals. Additionally, the predominant land-use class at each cell and its corresponding asset value are extracted. Asset value information for each cell is organized in a table based on land-use and water depth classes, with all values in the same table entry summed up. To calculate the direct damage, each asset value in the table is multiplied by the respective value of the specific damage function for the land-use class and water depth. The BEAM-specific damage functions developed for southern Germany, are adopted for this analysis (geomer GmbH and Ruiz Rodriguez + Zeisler + Blank GbR, 2020). The total direct damage for each inundation area is derived by summing all individual polygon damages. Given that inundation areas are delineated at 10 cm intervals for each dike segment (see Section 3.3), direct damages are available for every 10 cm of inundation elevation. Using the inundation volumes generated in the flood simulation model as an input, a linear interpolation is performed between these *V-D* data pairs to convert segment-specific inundation volumes into direct damages in a post-processing step, which is depicted in the lower panel of Fig. 9 for segment 500. This approach facilitates computationally efficient damage evaluations across numerous potential failure locations.

Based on the inundation areas of the river sections derived in the inundation module, damages are additionally estimated for river sections following the approach outlined for dike segments. As a result, every river section is associated with a W-D relation, where W denotes the water level in the river section. Flooding in the river section is treated as deterministic conditional on the maximum water level over all time steps resulting from the probabilistic breach analysis. If the river is bifuricated in the section, the lower, non-zero maximum water level of the two segments of a river section is taken as decisive. All damages, e.g., from river sections and dike segments, are summed up to obtain the total direct damage of the simulation run.



390

395

400

405



Following a comprehensive literature review (Sieg et al., 2019; Carrera et al., 2014; Olesen et al., 2017; de Bruijn et al., 2015; Pfurtscheller, 2014), indirect damages are estimated at 30% of the direct damages. Business interruption costs are also included at 30% of direct damages, based on recommendations of these studies. Hence, the direct damages are augmented by a total of $1.3 \cdot 1.3 = 1.69$. It is generally expected that indirect costs and business interruption expenses increase non-linearly with increasing damages; however, the extent of this relationship remains unclear and is influenced by various factors (Koks et al., 2015). Current methods for the comprehensive quantification of indirect damages and business interruption costs at large scale studies are still inadequate (Merz et al., 2010b), justifying the choice to employ two constant factors. Intangible damages are quantified in non-monetary terms, considering factors such as fatalities, natural reserves, critical infrastructure and drinking water protected areas. The reduction of risk associated with these factors is communicated as an additional benefit of the measures implemented, but it is not included in the formal benefit-cost analysis.

3.6 Model Implementation

The developed flood risk model differs from other methodologies, such as those presented by Vorogushyn (2008) and Domeneghetti et al. (2013), primarily in that the flood simulation model is executed independently of a coupling with hydraulic and hydrodynamic simulation models. This approach enhances computational efficiency while explicitly modeling the effects of the flood process components and their interactions. This enables its incorporation into a comprehensive uncertainty analysis framework, as outlined in the next section. The computational cost of the flood simulation model is on average 0.76 seconds per run (8-thread, 2.8 GHz CPU, no explicit parallelization). This cost scales approximately linearly with the number of breaches. A schematic representation of the model's architecture, implemented in a Matlab environment, is provided in Fig. 10, illustrating the workflow that is executed during each simulation run.

4 Uncertainty modeling

Flood risk models and their parameters have uncertainties. It is essential to acknowledge and communicate them, particularly in a decision-making context. Generally, uncertainties can be categorized into two types: aleatory and epistemic (Hall and Solomatine, 2008). Aleatory uncertainties refer to the inherent natural variability or randomness within the flood process that cannot be reduced by the modeler. By contrast, epistemic uncertainties denote the uncertainties associated with the model and its input data, which can potentially be reduced. Thus, it is imperative, especially within a decision-making context, to quantify the impact of epistemic model uncertainties on the relevant decision parameter(s). For that purpose, the flood risk model is embedded in a 2-level Monte Carlo framework, which is enabled by its low computational costs.

415 4.1 2-level Monte Carlo framework

Here, $Y = \mathcal{Y}(\mathbf{X})$ denotes the outcome of the flood simulation model, i.e. the damage estimate associated with a single flood event, with aleatory and epistemic uncertain input parameters $\mathbf{X} = [\mathbf{X}_a, \mathbf{X}_e]$, which are modeled as random variables. \mathbf{X}_a is a set of multiple hundreds of aleatory random variables, which represent the flood scenarios, the resistance of all dike segments





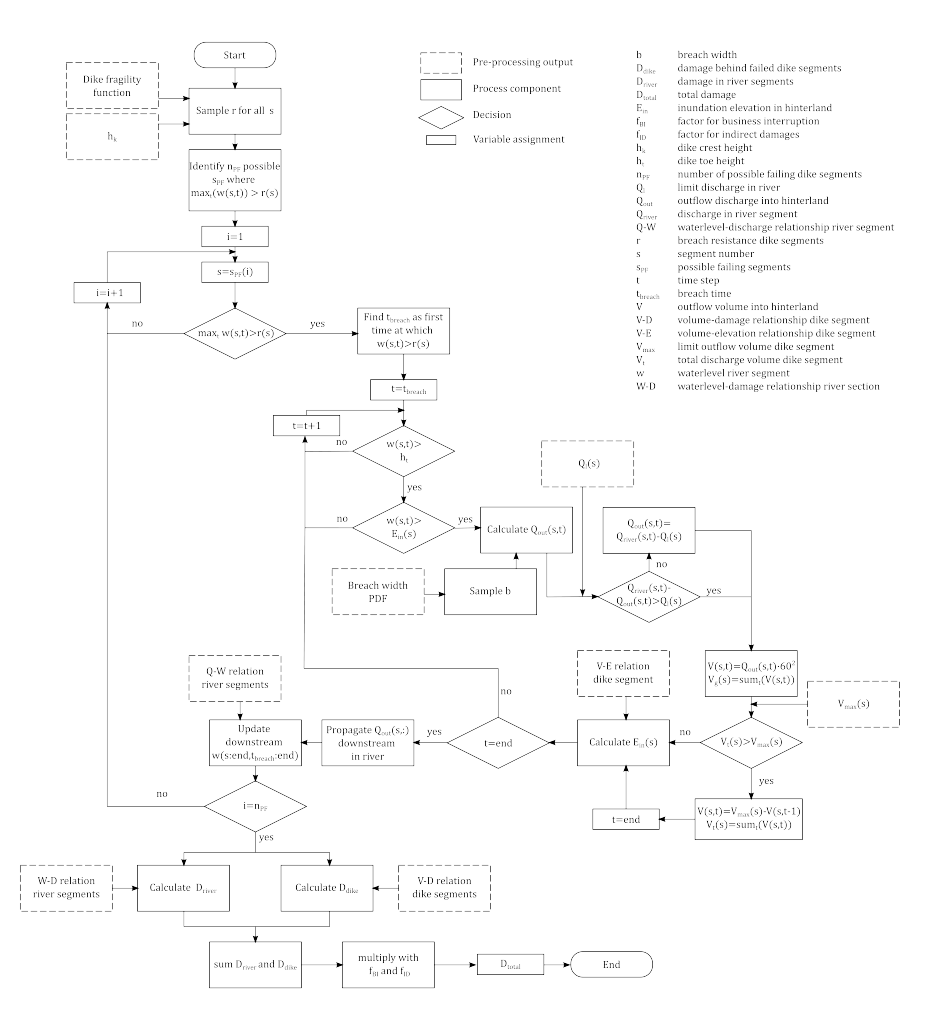


Figure 10. Process diagram of flood simulation model. Schematically shown is the procedure for one Monte Carlo run.

and the breach widths of failed dike segments. Given the large number of aleatory random variables and the strong non-linearity of the model result with respect to \mathbf{X}_a , the expectation of the damage conditional on \mathbf{X}_e is evaluated through a first-level Monte Carlo analysis with $n_{MC_a}=3600$ samples:

$$\mathcal{Y}_{e}(\mathbf{X}_{e} = \mathbf{x}_{e}) = \mathbb{E}_{\mathbf{X}_{a} | \mathbf{X}_{e} = \mathbf{x}_{e}} [\mathcal{Y}([\mathbf{X}_{e} = \mathbf{x}_{e}, \mathbf{X}_{a}])]$$

$$\approx \frac{1}{n_{MC_{a}}} \sum_{j=1}^{n_{MC_{a}}} \mathcal{Y}(\mathbf{X}_{e} = \mathbf{x}_{e}, \mathbf{x}_{a}^{(j)}),$$
(13)

The epistemic uncertainty is represented by 13 random variables \mathbf{X}_e , listed in Table 1. They are modeled by beta distributions and incorporated through a second-level Monte Carlo analysis with $n_{MC_e}=200$ samples. For each quasi-random realization of \mathbf{X}_e , the first-level analysis is performed. The expected damage over all simulation runs is estimated as:





$$\mathbb{E}_{\mathbf{X}}[\mathcal{Y}(\mathbf{X})] = \mathbb{E}_{\mathbf{X}_e}[\mathcal{Y}_e(\mathbf{X}_e)]$$

$$\approx \frac{1}{n_{MC_e}} \sum_{k=1}^{n_{MC_e}} \mathcal{Y}_e(\mathbf{x}_e^{(k)}).$$
(14)

The separation of aleatory and epistemic uncertainties is described in more detail in Straub et al. (2025).

430 4.2 Risk and benefit estimation

Ultimately, the flood risk model is developed to quantify the expected benefit of implementing individual or combined mitigation measures. The risk reduction associated with a measure M is defined as

$$\Delta r(a_M) = r(a_0) - r(a_M) \tag{15}$$

where a denotes a decision variable: a_0 represents the baseline scenario without additional mitigation, and a_M corresponds to the implementation of measure M. The annual flood risk under decision a, r(a), is computed as

$$r(a) = \lambda \cdot \mathbb{E}_{\mathbf{X}}[\mathcal{Y}(\mathbf{X}, a)],\tag{16}$$

We remind that $\lambda = 72/3500$ is the rate of flood events. The benefit $B(a_M)$ is defined as the sum of the discounted annual risk reduction $\Delta r(a_M)$ over the operational lifetime of the measure t_o

$$B(a_M) = \Delta r(a_M) \cdot \frac{1 - (1 + r_d)^{-t_o}}{r_d},\tag{17}$$

with r_d the annual discount rate. Based on the damage samples $\mathbf{Y} = \mathcal{Y}(\mathbf{X})$ resulting from the MC-based flood simulation, a loss exceedance curve can be derived. Therefore, the samples are ordered based on their damage estimate $Y_1 \geq Y_2 \geq ... \geq Y_{n_{MC_a}}$. The exceedance probability of each damage Y_i is calculated as

$$P(Y \ge Y_i) = i \cdot \frac{72}{3500 \cdot n_{MC}} \tag{18}$$

This is shown in Fig. 12 for a_0 , no measure, and the implementation of the measure under study, a_M . The area in between the two curves corresponds to the expected annual risk reduction in Eq. 15 (Arnel, 1989). To calculate the benefit-cost ratio of a measure, the benefit $B(a_M)$ is compared against the sum of discounted costs.

4.3 Sensitivity analysis

Sensitivity analysis generally aims at explaining how variations in model outputs can be attributed to uncertainties in input parameters (Pianosi et al., 2016). In this study, first-order Sobol' indices are calculated as a byproduct of the uncertainty analysis. They offer insights into the relative importance of parameter uncertainties, calculated as the direct contribution of each input parameter to the output variance

$$S_{X_{e,i}} = \frac{\operatorname{Var}(\mathbb{E}[Y_e|X_{e,i}])}{\operatorname{Var}(Y_e)}.$$
(19)





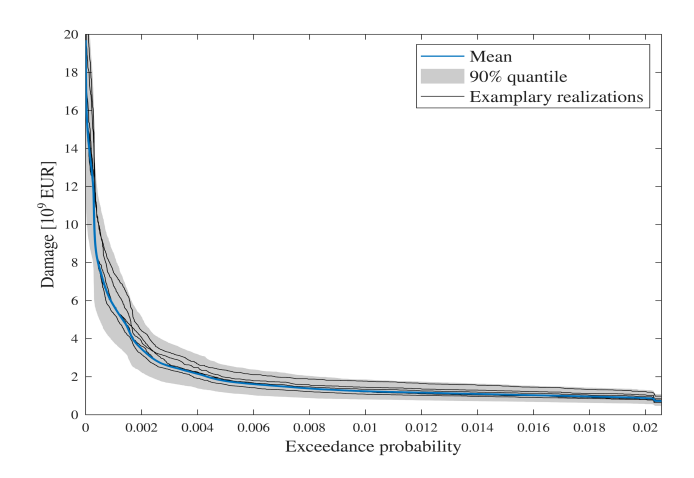


Figure 11. Loss exceedance curve at entire Bavarian Danube. Mean (blue), 90% quantile (grey) and five randomly selected loss exceedance curves given fixed epistemic parameters.

Since aleatory uncertainty cannot be reduced, quantifying the sensitivity with respect to all uncertainties $\mathbf{X} = [\mathbf{X}_a, \mathbf{X}_e]$ is not expedient, especially in a decision making context. Therefore, the sensitivity analysis considers as input only the epistemic uncertainties \mathbf{X}_e and as output the expected value of $\mathcal{Y}(\mathbf{X},a)$ with respect to the aleatory uncertainties \mathbf{X}_a , $Y_e = \mathcal{Y}_e(\mathbf{X}_e = \mathbf{x}_e)$, 455 estimated in Eq. 13. To approximate $\mathbb{E}[Y_e|X_{e,i}]$ based on the samples, a one-dimensional linear regression \mathcal{S} is applied, which is depicted in Fig. 14 for three uncertainties. If the absolute influence of parameter uncertainties on a specific decision is of interest, the expected value of partial perfect information (EVPPI) (Straub et al., 2025) is a more suitable metric. EVPPI quantifies the expected monetary benefit of making an improved decision, assuming perfect information about a specific uncertain input X_e . It can be used to assess whether it is worthwhile to invest in reducing uncertainty in a particular input parameter, or to identify which uncertainties should be prioritized in further analysis or data collection.

5 Results

460

465

Due to ongoing work on the climate inputs, the following results are preliminary. In this study, a total of $n_{MC} = n_{MC_a} \cdot n_{MC_e} = n_{MC_a} \cdot n_{MC_e}$ $3600 \cdot 200 = 720,000$ Monte Carlo simulation runs are performed. The samples are used to derive the expected loss exceedance curve at the Bayarian Danube, shown in blue in Fig. 11. The sampling process follows the 2-level framework outlined in Section 4.1 that enables the distinction between the influence of aleatory and epistemic uncertainties. The impact of epistemic uncertainties is represented by the 90% quantile in Fig. 11. Five loss exceedance curves, selected randomly from the $n_E = 200$ second-order simulation runs, are depicted in black to illustrate the effect of epistemic model uncertainties. As apparent from Fig. 11, the influence of model uncertainties is more pronounced for larger, less frequent damage events.

The developed flood risk model is further applied to quantify the flood risk reduction potential $\Delta r(a_M)$ of a controlled 470 detention basin located near Riedensheim at the Bavarian Danube. It fits a volume of around $8 \cdot 10^6 \, \mathrm{m}^3$ with a maximum intake capacity of 170 m³/s. Its operating mode is directly included in the flood simulation model and follows predefined rules





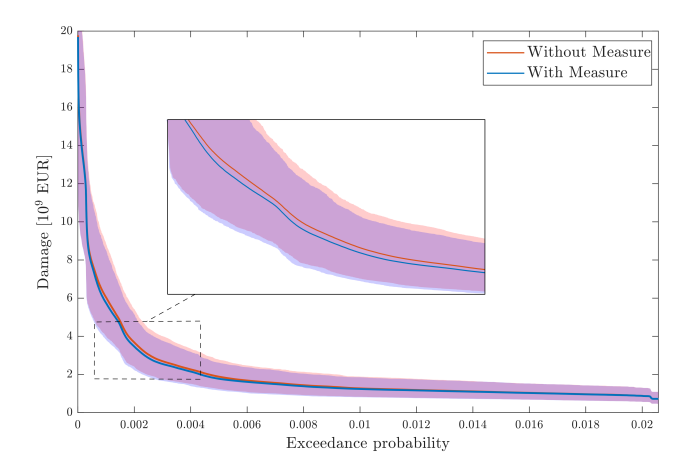


Figure 12. Loss exceedance curve at Bavarian Danube with (blue) and without (red) mitigation measure. Respective 90% quantile shown as shaded area.

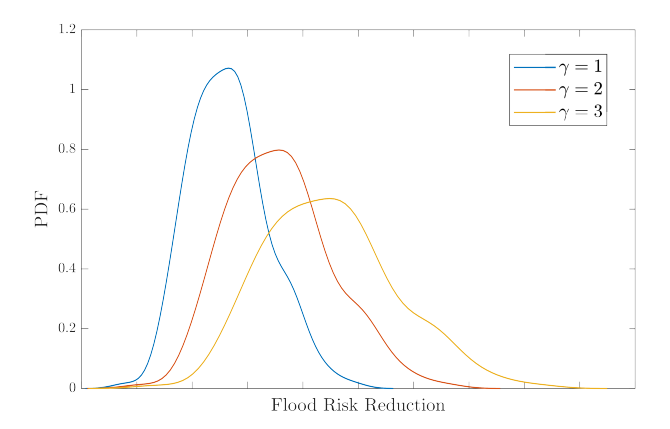


Figure 13. Probability distribution (PDF) of the annual flood risk reduction at the Bavarian Danube achieved by the detention basin. The blue PDF corresponds to the assumption of a constant climate, the red PDF to a linear increase in flood frequency until 2120 by a factor $\gamma=2$ and the yellow PDF to an flood frequency increase by a factor of $\gamma=3$. No numbers are shown on the x-axis due to the preliminary nature of the results.

assuming perfect forecasts. The resulting preliminary loss exceedance curve is presented in blue in Fig. 12. As outlined in Section 4.2, the annual risk reduction is equivalent to the area between the two loss exceedance curves.

Kernel-smoothing is applied to estimate the probability density function (PDF) of the annual risk reduction, which is depicted in blue in Fig. 13. No numerical values are provided as the result is preliminary. To incorporate these results into a benefit-cost analysis, the expected annual flood risk reduction over the projected lifetime of the measure is discounted relative to the reference year, summed, and compared to the discounted costs of the measure, as described in section 4.2.



490



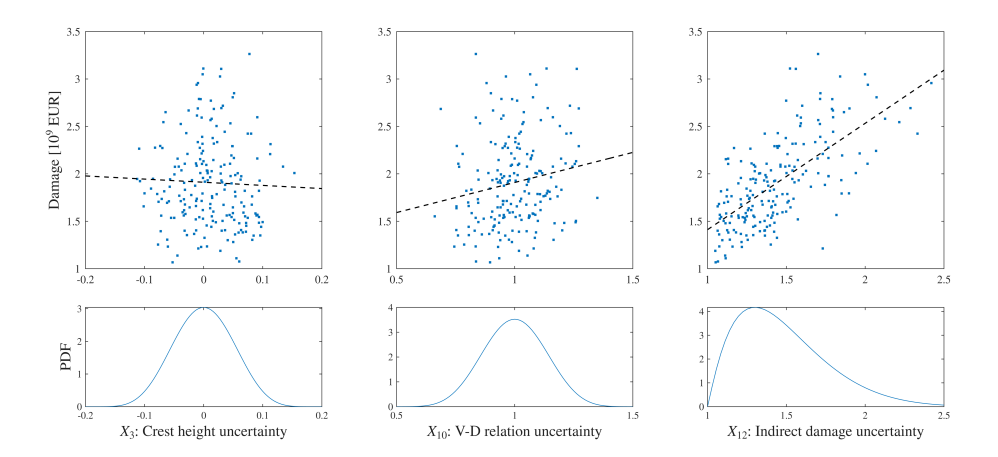


Figure 14. Scatter plot of the influence of three epistemic uncertain parameters on the expected damage and their assigned underlying beta distribution.

The $n_{ep}=13$ epistemic model uncertainties are listed in Table 1. A comprehensive presentation of all 13 model uncertainty factors is omitted here. Instead, we focus on three selected factors, namely the uncertainty in the dike crest heights X_3 , modeled by an additive factor; the uncertainty in the V-D relation X_{10} , modeled by a multiplicative factor; and the indirect damage X_{12} , represented as a proportion of direct damage. The distributions of these three model uncertainty factors are illustrated in blue in Fig. 14. The expected damages with respect to the aleatory uncertainties, $\mathbb{E}_{\mathbf{X}_a|\mathbf{X}_e=\mathbf{x}_e}[\mathcal{Y}([\mathbf{X}_e=\mathbf{x}_e,\mathbf{X}_a])]$, are plotted against the sampled factor values $X_3=x_3$, $X_{10}=x_{10}$, and $X_{13}=x_{13}$ in the same Fig.. The substantial influence of the indirect damage factor on the overall damage is clearly evident. Additionally, a formal variance-based sensitivity analysis is conducted, and the first-order Sobol' indices are provided in Table 1.

The results of the sensitivity analysis suggest that the uncertainty of parameters entering the damage module has the greatest impact on the expected flood damages and, consequently, the annual flood risk. This finding supports the conclusions of Apel et al. (2009a), who noticed that the choice of the flood damage model has a more significant impact on the flood risk estimate than the parameters within the flood simulation model, emphasizing the need for further development of the damage module. The uncertainties inherent in the hydrological load module are not incorporated in this uncertainty analysis. To assess the impact of an expected climate change based increase in flood frequency on the risk reduction potential, a scenario analysis is conducted. The occurrence rate of a flood $\lambda = 72/3500$ years⁻¹ is linearly increased until the year 2120 by a factor γ

$$\hat{\lambda}(t) = \frac{\gamma - 1}{t_o} \cdot t \cdot \lambda \quad \text{for } t \in [0, t_o]$$
 (20)

The influence of γ on the distribution of annual flood risk reduction is illustrated in Fig. 13 for the two scenarios $\gamma = 2$ and $\gamma = 3$. An increased flood occurrence rate leads to larger expected flood risk reduction, and consequently a higher benefit of the detention basin; however, this also results in increased uncertainty.





Table 1. Quantified uncertain parameters and their first order Sobol' indices.

	Uncertainty	Sobol' index
X_1	Fragility function	0
X_2	Q-W relation river segments	0.02
X_3	Dike crest height	0.05
X_4	Discharge reduction factor	0.01
X_5	Breach width PDF	0.01
X_6	Breach height	0.01
X_7	Limit discharge	0.01
X_8	Maximum outflow volume	0.02
X_9	V-E relation dike segment	0.04
X_{10}	V-D relation dike segment	0.13
X_{11}	W-D relation river section	0.06
X_{12}	Business interruption factor	0.16
X_{13}	Indirect damage factor	0.34

6 Concluding remarks

500

505

This work proposes a flood risk model to enable large-scale uncertainty-aware flood risk assessments for decision support on mitigation measures. The model is computationally efficient because it makes use of the results of different climatic, hydrodynamic and hydraulic simulations conducted in a pre-processing step. As a result, it does not depend on computationally intensive simulations during run time. A key element enabling this independence is the developed flood routing method, along with segment-specific lookup tables that store the relationships between inundation elevation, floodwater volume, and damages. This computational efficiency allows the model to be integrated into a two-level Monte Carlo framework for uncertainty quantification. Within this framework, different types of uncertainty — aleatory and epistemic — are treated separately. This separation allows for the isolated examination of epistemic uncertainties, helping to understand the influence of various model uncertainties and make targeted improvements. Furthermore, the separation ensures that the estimated benefits of mitigation measures remain robust across a wide range of possible flood events and failure scenarios. Especially in the context of natural hazards like floods, which are characterized by high aleatory uncertainty, it is essential to quantify, communicate, and incorporate this uncertainty into the decision-making process. The literature review in Section 1 highlighted the inherent trade-offs in flood risk models between process representation, spatial coverage, and the integration within uncertainty analyses. The developed model enables both large-scale flood risk and benefit assessments as well as detailed uncertainty analyses. However, a compromise is made through simplifications that are necessary to allow pre-processing of parts of the model, which reduce the model's accuracy locally. Nevertheless, results of module verification and the uncertainty analysis suggest that the effect of these inaccuracies remains within an acceptable range, in particular when considering mitigation measures that act globally, https://doi.org/10.5194/egusphere-2025-4875 Preprint. Discussion started: 10 November 2025

© Author(s) 2025. CC BY 4.0 License.



530

EGUsphere Preprint repository

such as flood detention basins. Sensitivity analyses indicate that future improvements should focus on components of the damage assessment module. For applications to mitigation measures that act locally, integrating a more precise damage model for the affected region is possible due to the modular nature of the model framework.

The developed model provides a solid foundation for decision-making, such as in benefit-cost analyses. In an ongoing study, it is being applied to the Bavarian Danube in Germany to evaluate the benefit of a flood mitigation measure, along with its associated uncertainties. In the future, the model can support assessments of various mitigation strategies, help identify high-risk areas, or optimize the combination of mitigation measures. In this way, the model contributes to the advancement of integrated flood risk management. It demonstrates how dynamic, probabilistic, and integrated flood risk management can be implemented in practice. We hope that our work encourages and supports decision-makers in moving toward a more holistic approach to flood risk management.

Code availability. The main code of the flood simulation model is available at https://github.com/mara-tum/flood-risk-model.git

Data availability. The data used in this study are provided by Bayerisches Landesamt für Umwelt (LfU) and cannot be published.

Author contributions. All authors contributed to the conceptual design of the model. The model was developed mainly by MR, with input from AH, under the guidance of DS. MR performed the numerical investigations, AH prepared most of the data input. MR wrote the manuscript, AH and DS revised it.

Competing interests. The authors declare that they have no conflict of interest.

Acknowledgements. We thank Bayerisches Landesamt für Umwelt (LfU) and Bayerisches Staatsministerium für Umwelt und Verbraucherschutz (StMUV) for the fruitful discussions. The LfU also provided the discharge inputs of the flood scenarios used in the case study.





References

555

- Apel, H., Thieken, A. H., Merz, B., and Blöschl, G.: Flood risk assessment and associated uncertainty, Natural Hazards and Earth System Sciences, 4, 295–308, https://doi.org/10.5194/nhess-4-295-2004, 2004.
 - Apel, H., Thieken, A. H., Merz, B., and Blöschl, G.: A Probabilistic Modelling System for Assessing Flood Risks, Natural Hazards, 38, 79–100, https://doi.org/10.1007/s11069-005-8603-7, 2006.
- Apel, H., Aronica, G. T., Kreibich, H., and Thieken, A. H.: Flood risk analyses—how detailed do we need to be?, Natural Hazards, 49, 79–98, https://doi.org/10.1007/s11069-008-9277-8, 2009a.
 - Apel, H., Merz, B., and Thieken, A.: Influence of dike breaches on flood frequency estimation, Computers & Geosciences, 35, 907–923, https://doi.org/10.1016/j.cageo.2007.11.003, 2009b.
 - Arnel, N. W.: Expected Annual Damages and Uncertainties in Flood Frequency Estimation, Water Resources Planning and Management, 115, 94–107, https://doi.org/10.1061/(ASCE)0733-9496(1989)115:1(94), 1989.
- 545 Bremicker, M.: Das Wasserhaushaltsmodell LARSIM Modellgrundlagen und Anwendungsbeispiele, Freiburger Schriften zur Hydrologie, Institut für Hydrologie der Universität Freiburg i.Br., Freiburg i.Br., Deutschland, 2000.
 - Carrera, L., Standari, G., Bosello, F., and Mysiak, J.: Assessing Direct and Indirect Economic Impacts of a Flood Event Through the Integration of Spatial and Computational General Equilibrium Modelling, Environmetal Modeling and Software, 63, 109–122, https://www.jstor.org/stable/resrep01092, 2014.
- Curran, A., de Bruijn, K., Klerk, W., and Kok, M.: Large Scale Flood Hazard Analysis by Including Defence Failures on the Dutch River System, Water, 11, 1732, https://doi.org/10.3390/w11081732, 2019.
 - Curran, A., de Bruijn, K., Domeneghetti, A., Bianchi, F., Kok, M., Vorogushyn, S., and Castellarin, A.: Large-scale stochastic flood hazard analysis applied to the Po River, Natural Hazards, 104, 2027–2049, https://doi.org/10.1007/s11069-020-04260-w, 2020.
 - CUR/TAW: Probabilistic design of flood defences. Report 141., Technical Advisory Committee on Water Defences, Center for Civil Engineering Research and Codes, Gouda, Netherlands, 1990.
 - de Bruijn, K., Wagenaar, D., Slager, K., de Bel, M., and Burzel, A.: Updated and improved method for flood damage assessment: SSM2015 (version 2), Tech. rep., Deltares, 2015.
 - de Kok, J.-L. and Grossmann, M.: Large-scale assessment of flood risk and the effects of mitigation measures along the Elbe River, Natural Hazards, 52, 143–166, https://doi.org/10.1007/s11069-009-9363-6, 2010.
- de Moel, H., Jongman, B., Kreibich, H., Merz, B., Penning-Rowsell, E., and Ward, P. J.: Flood risk assessments at different spatial scales, Mitigation and Adaptation Strategies for Global Change, 20, 865–890, https://doi.org/10.1007/s11027-015-9654-z, 2015.
 - Deltares: SOBEK. Hydrodynamics, Rainfall Runoff and Realtime Control. User Manual, Tech. rep., 2018.
 - Dittes, B., Špačková, O., Schoppa, L., and Straub, D.: Managing uncertainty in flood protection planning with climate projections, Hydrology and Earth System Sciences, 22, 2511–2526, https://doi.org/10.5194/hess-22-2511-2018, 2018.
- Domeneghetti, A., Vorogushyn, S., Castellarin, A., Merz, B., and Brath, A.: Probabilistic flood hazard mapping: effects of uncertain boundary conditions, Hydrology and Earth System Sciences, 17, 3127–3140, https://doi.org/10.5194/hess-17-3127-2013, 2013.
 - Förster, S., Kneis, D., Gocht, M., and Bronstert, A.: Flood risk reduction by the use of retention areas at the Elbe River, International Journal of River Basin Management, 3, 21–29, https://doi.org/10.1080/15715124.2005.9635242, 2005.
- Gamper, C. D., Thöni, M., and Weck-Hannemann, H.: A conceptual approach to the use of Cost Benefit and Multi Criteria Analysis in natural hazard management, Natural Hazards and Earth System Sciences, 6, 293–302, https://doi.org/10.5194/nhess-6-293-2006, 2006.



580



- geomer GmbH and Ruiz Rodriguez + Zeisler + Blank GbR: Bewertung des Hochwasserrisikos auf der Grundlage von Schadenspotenzialen Anwendung von Schadensfunktionen in repräsentativen Beispielsregionen im Rahmen des Länderfinanzierungsprogramms "Wasser, Boden und Abfall", Tech. rep., 2020.
- Gouldby, B., Sayers, P., Mulet-Marti, J., Hassan, M. A. A. M., and Benwell, D.: A methodology for regional-scale flood risk assessment,

 Proceedings of the Institution of Civil Engineers Water Management, https://doi.org/10.1680/wama.2008.000.0.1, 2008.
 - Hall, J. and Solomatine, D.: A framework for uncertainty analysis in flood risk management decisions, International Journal of River Basin Management, 6, 85–98, https://doi.org/10.1080/15715124.2008.9635339, 2008.
 - Hall, J. W., Dawson, R. J., Sayers, P. B., Rosu, C., Chatterton, J. B., and Deakin, R.: A methodology for national-scale flood risk assessment, Proceedings of the Institution of Civil Engineers Water and Maritime Engineering, 156, 235–247, https://doi.org/10.1680/wame.2003.156.3.235, 2003.
 - IPCC: Summary for Policymakers, Cambridge University Press, United Kingdom and New York, USA, 2013.
 - Kamrath, P., Disse, M., Hammer, M., and Köngeter, J.: Assessment of Discharge through a Dike Breach and Simulation of Flood Wave Propagation, Natural Hazards, 38, 63–78, https://doi.org/10.1007/s11069-005-8600-x, 2006.
- Koks, E. E., Bočkarjova, M., de Moel, H., and Aerts, J. C. J. H.: Integrated Direct and Indirect Flood Risk Modeling: Development and Sensitivity Analysis, Risk Analysis, 35, 882–900, https://doi.org/10.1111/risa.12300, 2015.
 - Ludwig, R., Wood, R. R., Willkofer, F., Mittermeier, M., Böhnisch, A., and Poschlod, B.: Klimawandel und Extremereignisse. Risiken und Perspektiven für die Bayerische Wasserwirtschaft. Abschlussbericht, München, Germany, 2019.
 - Merz, B. and Thieken, A. H.: Flood risk curves and uncertainty bounds, Natural Hazards, 51, 437–458, https://doi.org/10.1007/s11069-009-9452-6, 2009.
- 590 Merz, B., Hall, J., Disse, M., and Schumann, A.: Fluvial flood risk management in a changing world, Natural Hazards and Earth System Sciences, 10, 509–527, https://doi.org/10.5194/nhess-10-509-2010, 2010a.
 - Merz, B., Kreibich, H., Schwarze, R., and Thieken, A.: Review article 'Assessment of economic flood damage', Natural Hazards and Earth System Sciences, 10, 1697–1724, https://doi.org/10.5194/nhess-10-1697-2010, 2010b.
- Messner, F., Penning-Rowsell, E., Green, C., Meyer, V., Tunstall, S., and Veen, A.: Evaluating flood damage: guidance and recommendations on principles and methods, Tech. rep., FLOOD Site Project Report, 2007.
 - Metin, A. D., Dung, N. V., Schröter, K., Guse, B., Apel, H., Kreibich, H., Vorogushyn, S., and Merz, B.: How do changes along the risk chain affect flood risk?, Natural Hazards and Earth System Sciences, 18, 3089–3108, https://doi.org/10.5194/nhess-18-3089-2018, 2018.
 - Olesen, L., Löwe, R., and Arnbjerb-Nielsen, K.: Flood Damage Assessment. Literature review and recommended procedure, Tech. rep., Cooperative Research Centre for Water Sensitive Cities, Melbourne, Australia, 2017.
- Petrow, T., Thieken, A. H., Kreibich, H., Merz, B., and Bahlburg, C. H.: Improvements on Flood Alleviation in Germany: Lessons Learned from the Elbe Flood in August 2002, Environmental Management, 38, 717–732, https://doi.org/10.1007/s00267-005-6291-4, 2006.
 - Pfurtscheller, C.: Regional economic impacts of natural hazards the case of the 2005 Alpine flood event in Tyrol (Austria), Natural Hazards and Earth System Sciences, 14, 359–378, https://doi.org/10.5194/nhess-14-359-2014, 2014.
- Pianosi, F., Beven, K., Freer, J., Hall, J. W., Rougier, J., Stephenson, D. B., and Wagener, T.: Sensitivity analysis of environmental models: A systematic review with practical workflow, Environmental Modelling & Software, 79, 214–232, https://doi.org/10.1016/j.envsoft.2016.02.008, 2016.
 - Sairam, N., Brill, F., Sieg, T., Farrag, M., Kellermann, P., Nguyen, V. D., Lüdtke, S., Merz, B., Schröter, K., Vorogushyn, S., and Kreibich, H.: Process-Based Flood Risk Assessment for Germany, Earth's Future, 9, e2021EF002259, https://doi.org/10.1029/2021EF002259, 2021.



615

620



- Schulla, J. and Jasper, K.: Model description WaSiM-ETH, Zürich, Switzerland, 2007.
- 610 Schultz, M. T., Gouldby, B. P., Simm, J. D., and Wibowo, J. L.: Beyond the Factor of Safety: Developing Fragility Curves to Characterize System Reliability:, Tech. rep., Defense Technical Information Center, Fort Belvoir, VA, https://doi.org/10.21236/ADA525580, 2010.
 - Sieg, T., Schinko, T., Vogel, K., Mechler, R., Merz, B., and Kreibich, H.: Integrated assessment of short-term direct and indirect economic flood impacts including uncertainty quantification, PLOS ONE, 14, e0212 932, https://doi.org/10.1371/journal.pone.0212932, 2019.
 - Straub, D., Betz, W., Ruf, M., Hoffmann, A., Landgraf, A., Friedli, L., and Papaioannou, I.: Sensitivity measures for engineering and environmental decision support, https://arxiv.org/abs/2507.08488, 2025.
 - Thieken, A. H., Kienzler, S., Kreibich, H., Kuhlicke, C., Kunz, M., Mühr, B., Müller, M., Otto, A., Petrow, T., Pisi, S., and Schröter, K.: Review of the flood risk management system in Germany after the major flood in 2013, Ecology and Society, 21, art51, https://doi.org/10.5751/ES-08547-210251, 2016.
 - Thomas, F. and Knüppe, K.: From Flood Protection to Flood Risk Management: Insights from the Rhine River in North Rhine-Westphalia, Germany, Water Resources Management, 30, 2785–2800, https://doi.org/10.1007/s11269-016-1323-9, 2016.
 - USACE: Benefit determination involving existing levees. Policy Guide Letter 26. Memorandum for Major Subordinate Commands and District Commands., Tech. rep., U.S. Army Corps of Engineering, 1991.
 - Vitale, C.: Understanding the shift toward a risk-based approach in flood risk management, a comparative case study of three Italian rivers, Environmental Science & Policy, 146, 13–23, https://doi.org/10.1016/j.envsci.2023.04.015, 2023.
- 625 Vorogushyn, S.: Analysis of flood hazard under consideration of dike breaches, Ph.D. thesis, Universität Potsdam, 2008.
 - Vorogushyn, S., Merz, B., Lindenschmidt, K., and Apel, H.: A new methodology for flood hazard assessment considering dike breaches, Water Resources Research, 46, 2009WR008475, https://doi.org/10.1029/2009WR008475, 2010.